Theoretical and Applied Mechanics Letters 11 (2021) 100248

Contents lists available at ScienceDirect

Theoretical and Applied Mechanics Letters

journal homepage: www.elsevier.com/locate/taml

Letter

Error of large-eddy simulation in the wall pressure fluctuation of a turbulent channel flow

Rong Li[a,b], Bowen Yang[a], Zixuan Yang[a,b,*], Shizao Wang[a,b], Guowei He[a,b]

[a] State Key Laboratory of Nonlinear Mechanics, Institute of Mechanics, Chinese Academy of Sciences, Beijing 100190, China
[b] School of Engineering Sciences, University of Chinese Academy of Sciences, Beijing 100049, China

ARTICLE INFO

Article history:
Received 1 March 2021
Revised 24 March 2021
Accepted 29 March 2021
Available online 20 April 2021

Keywords:
Wall pressure
Large-eddy simulation
Turbulent channel flow

ABSTRACT

We analyze the error of large-eddy simulation (LES) in wall pressure fluctuation of a turbulent channel flow. To separate different sources of the error, we conduct both direct numerical simulations (DNS) and LES, and apply an explicit filter on DNS data to obtain filtered DNS (FDNS) data. The error of LES is consequently decomposed into two parts: The first part is the error of FDNS with respect to DNS, which quantifies the influence of the filter operation. The second part is the difference between LES and FDNS induced by the error of LES in velocity field. By comparing the root-mean-square value and the wavenumber-frequency spectrum of the wall pressure fluctuation, it is found that the inaccuracy of the velocity fluctuations is the dominant source that induces the error of LES in the wall pressure fluctuation. The present study provides a basis on future LES studies of the wall pressure fluctuation.

An accurate prediction of wall pressure fluctuations is a basis for the investigation of noise generation and flow-induced vibration in many engineering applications [1,2]. In literature, there are extensive experimental and theoretical studies of the wall pressure, and comprehensive reviews are given by Willmarth [3] and Eckelmann [4].

During the last two decades, numerical simulation becomes increasingly important in turbulence research. Among various simulation strategies, the direct numerical simulation (DNS) provides an accurate prediction of the wall pressure fluctuations [5–8]. However, the computational cost of DNS increases at a rate of the cube of the Reynolds number [9], and therefore, the application of DNS is limited to flows at low and moderate Reynolds numbers. The large eddy simulation (LES) uses grid to resolve large-scale motions of turbulence with the influences of the unresolved motions represented by a subgrid-scale model. LES is less expensive than DNS, and is therefore expected to become a useful tool for engineering applications. Viazzo et al. [10] used LES to study the statistics and spectra of the wall pressure fluctuations in turbulent channel flow at $Re_\tau = 640$. Park and Moin [11] reported the space-time characteristics of the wall pressure fluctuations using wall-modeled LES of a turbulent channel flow at $Re_\tau = 2000$. They noted that the resolution required for an accurate prediction of the wall pressure fluctuations was more stringent than that of the velocity field. In the above LES studies of the wall pressure fluctuations, although some features of the wall pressure fluctuations are captured qualitatively, the error is non-negligible.

In an incompressible turbulent channel flow, the pressure is governed by the following Poisson equation and boundary conditions

$$\frac{1}{\rho}\frac{\partial^2 p}{\partial x_k \partial x_k} = f = -\frac{\partial u_i}{\partial x_j}\frac{\partial u_j}{\partial x_i},$$
$$\frac{\partial p}{\partial x_2}(x_2 = \pm h) = \nu\frac{\partial^2 u_2}{\partial x_2^2}, \tag{1}$$

where p denotes the pressure, u_i is the velocity, with the subscript $i = 1, 2$, and 3 being the streamwise, wall-normal, and spanwise directions, respectively, ρ and ν represent the density and kinematic viscosity, respectively, $x_2 = \pm h$ represents the locations of two solid walls, and h is one-half the channel height. Filtering Eq. (1) results in the governing equation of the resolved pressure as

$$\frac{1}{\rho}\frac{\partial^2 \overline{p}}{\partial x_k \partial x_k} = \overline{f} = -\overline{\frac{\partial u_i}{\partial x_j}\frac{\partial u_j}{\partial x_i}},$$
$$\frac{\partial \overline{p}}{\partial x_2}(x_2 = \pm h) = \nu\frac{\partial^2 \overline{u}_2}{\partial x_2^2}, \tag{2}$$

* Corresponding author.
E-mail address: yangzx@imech.ac.cn (Z. Yang).

https://doi.org/10.1016/j.taml.2021.100248

Table 1
Number of grid points N_i and grid resolution Δx_i for DNS and LES of turbulent channel flow at $Re_\tau = 550$.

	$N_1 \times N_2 \times N_3$	$\Delta x_1{}^+$	$\Delta x_2{}^+$	$\Delta x_3{}^+$
DNS	$576 \times 256 \times 576$	12.0	0.04–6.75	6.0
LES	$96 \times 64 \times 96$	72.0	0.66–27.0	36.0

where the overline denotes a filtering operation. In LES, only the resolved part of u_i is available, and as such the pressure can be only calculated approximately by solving the following equation

$$\frac{1}{\rho}\frac{\partial^2 \overline{p}}{\partial x_k \partial x_k} = \overline{f} = -\overline{\frac{\partial \overline{u}_i}{\partial x_j}\frac{\partial \overline{u}_j}{\partial x_i}},$$
$$\frac{\partial \overline{p}}{\partial x_2}(x_2 = \pm h) = \nu \frac{\partial^2 \overline{u}_2}{\partial x_2^2}, \tag{3}$$

where the velocity in the source term of Eq. (2) is replaced by the resolved velocity $\bar{u}_i$. By contrasting Eqs. (2) and (3), it is understood that the error of LES in the pressure (with respect to the DNS result) indeed consists of two parts. The first part is induced by the filter, or equivalently, by the difference between u_i and $\bar{u}_i$. The second part is caused by the inaccuracy of LES in the resolved velocity $\bar{u}_i$, or equivalently, by the difference between DNS and LES in $\bar{u}_i$.

In the present study, we aim to find the dominate source of the error of LES in the wall pressure fluctuations. For this purpose, we conduct both DNS and LES of a turbulent channel flow, and filter the DNS data to obtain filtered DNS (FDNS) data. The error induced by the filter is estimated by comparing the solutions of Eqs. (2) and (3), in which u_i and $\bar{u}_i$ are given by DNS and FDNS, respectively. The error caused by the inaccuracy of LES in $\bar{u}_i$ is quantified by comparing the solutions of Eq. (3) between FDNS and LES.

To collect data needed for the analyses of the error of LES in the wall pressure fluctuation, both DNS and LES of turbulent channel flows are conducted. The Reynolds number is set to $Re_b = u_b h/\nu = 10150$, where u_b is the bulk mean velocity. The corresponding Reynolds number based on the wall friction velocity u_τ is $Re_\tau = u_\tau h/\nu = 550$. The flow is driven by a streamwise pressure gradient, which is adjusted to sustain a constant value of the bulk mean velocity u_b. Periodic boundary conditions are adopted in the streamwise and spanwise directions, while no-slip and no-penetration conditions are prescribed at two solid walls. The computational domain is set to $L_1 \times L_2 \times L_3 = 4\pi h \times 2h \times 2\pi h$. For spatial discretization, all flow quantities are expanded into Fourier series in the streamwise and spanwise directions, and into Chebychev polynomials in the wall-normal direction. A third-order time-splitting method [12] is utilized for time advancement. Table 1 summarizes the number of grid points N_i and grid resolution Δx_i of DNS and LES. The dynamic Smagorinsky model [13,14] is chosen to conduct LES.

To obtain the FDNS flow field, a sharp cut-off filter in the spectral space is applied. Below are the descriptions of the filter. The velocity field u_i of DNS is first expanded into coefficients of Fourier series and Chebyshev polynomials as

$$u_i(x_i,t) = \sum_{m=-\frac{1}{2}N_1}^{\frac{1}{2}N_1-1}\sum_{n=-\frac{1}{2}N_3}^{\frac{1}{2}N_3-1}\sum_{p=0}^{N_2}\tilde{u}_i(m,p,n,t) \times \exp[\mathrm{i}(m\alpha x_1 + n\beta x_3)]T_p(x_2), \tag{4}$$

where $\alpha = 2\pi/L_1$ and $\beta = 2\pi/L_3$ are the wavenumber resolutions in the streamwise and spanwise directions, respectively, $T_p(x_2)$ is the pth-order Chebyshev polynomial, and the tilde denotes the spectral coefficients of an arbitrary flow quantity. The spectral coefficients of velocity $\tilde{u}_i$ are then truncated to obtain the FDNS velocity, viz.

$$\bar{u}_i(x_i,t) = \sum_{m=-\frac{1}{2}N_1^f}^{\frac{1}{2}N_1^f-1}\sum_{n=-\frac{1}{2}N_3^f}^{\frac{1}{2}N_3^f-1}\sum_{p=0}^{N_2^f}\tilde{u}_i(m,p,n,t) \times \exp[\mathrm{i}(m\alpha x_1 + n\beta x_3)]T_p(x_2), \tag{5}$$

where N_i^f represents the number of grid points of the FDNS data, which is chosen to be consistent with that of LES (see Table 1) to facilitate a direct comparison of FDNS and LES results.

In the applications of the flow-induced vibration and noise, the wavenumber–frequency spectrum of wall pressure plays an important role. Therefore, we also examine the error of LES in the wavenumber–frequency spectrum of the wall pressure fluctuation, which is calculated using the method of Choi and Moin [6]. Specifically, a time series of the wall pressure fluctuation $p(x_1, x_3, t)$ is divided into intervals with 50% overlapping with the neighboring ones. Each time interval contains $N_s = 512$ time samples. The time length between two samples is $\Delta T_s^+ = 0.298$, which gives the highest frequency of $\omega_{\max}^+ = \pi/\Delta T_s^+ = 10.54$. In this paper, the superscript "+" is used to denote variables non-dimensionalized using the viscous lengthscale ν/u_τ and wall-friction velocity u_τ as characteristic length and velocity scales, respectively. Consequently, the time duration of each time interval is $T_l^+ = N_s \Delta T_s^+ = 152.6$, which corresponds to a frequency resolution of $\Delta\omega^+ = 2\pi/T_l^+ = 4.1 \times 10^{-2}$.

The wall pressure p in each interval is Fourier transformed in x_1 and x_3-directions and in time to obtain its Fourier coefficients $\hat{p}$ as

$$\hat{p}(k_1,k_3,\omega) = \frac{1}{L_1 L_3 \sqrt{T_l \int_0^{T_l} w^2(t)\mathrm{d}t}} \times \int_0^{T_l}\int_0^{L_1}\int_0^{L_3} w(t)p(x_1,x_3,t)\exp[\mathrm{i}(k_1x_1 + k_3x_3 + \omega t)]\mathrm{d}x_1\mathrm{d}x_3\mathrm{d}t, \tag{6}$$

where k_1 and k_3 are wavenumbers in the streamwise and spanwise directions, respectively, and $w(t)$ is a standard Hanning window function. The wavenumber–frequency spectrum of the wall pressure fluctuation $\Phi_{pp}(k_1,k_3,\omega)$ is then calculated as Eq. (7)

$$\Phi_{pp}(k_1,k_3,\omega) = \frac{1}{\alpha\beta\Delta\omega N_l}\sum \hat{p}(k_1,k_3,\omega)\hat{p}^*(k_1,k_3,\omega), \tag{7}$$

where the asterisk "*" denotes complex conjugate. The summation is performed over all time intervals, and N_l is the total number of time intervals. Taking the summation of $\Phi_{pp}(k_1,k_3,\omega)$ over k_3 yields the k_1–ω spectrum of the wall pressure fluctuation $\Phi_{pp}(k_1,\omega)$, viz.

$$\Phi_{pp}(k_1,\omega) = \sum_{k_3}\Phi_{pp}(k_1,k_3,\omega). \tag{8}$$

Figure 1 compares the profiles of the resolved mean velocity $\bar{U}_1^+$ and root-mean-square (RMS) velocity $\bar{u}_{i,rms}^+$ obtained from FDNS and LES. The corresponding full-scale values of U_1^+ and $u_{i,rms}^+$ obtained from DNS are also depicted. Note that due to the error of LES, the values of the wall friction velocity u_τ obtained from LES and DNS are different. To facilitate an unbiased comparison of the results, the value of u_τ obtained from DNS is used for non-dimensionalizing both DNS and LES results. It is seen from Fig. 1a that the profiles of U_1^+ and $\bar{U}_1^+$ obtained respectively from DNS and FDNS collapse, indicating that the filtering imposes little influence on the mean flow. The LES result of $\bar{U}_1^+$ is in reasonable agreement with the FDNS result, except for a slight underprediction in part of the logarithmic layer ($30 < x_2^+ < 180$). Figure 1b shows that in the buffer layer ($5 < x_2^+ < 30$), where turbulence is intensive, the magnitudes of all three components of the resolved RMS velocity $\bar{u}_{i,rms}^+$ of FDNS are smaller than those of the corresponding full-scale RMS velocity $u_{i,rms}^+$ of DNS, because the small-scale motions are filtered

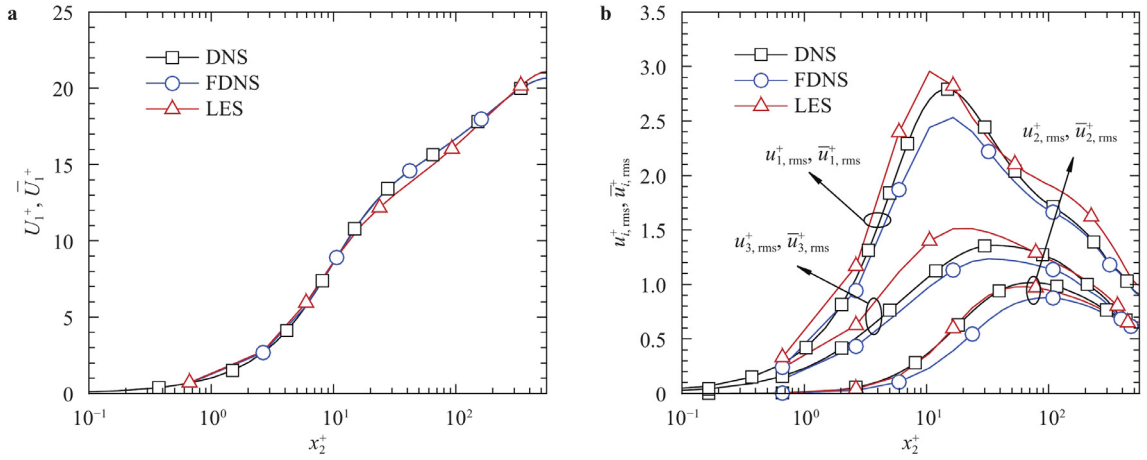

Fig. 1. Profiles of a mean streamwise velocity and b RMS velocity obtained from DNS, FDNS, and LES.

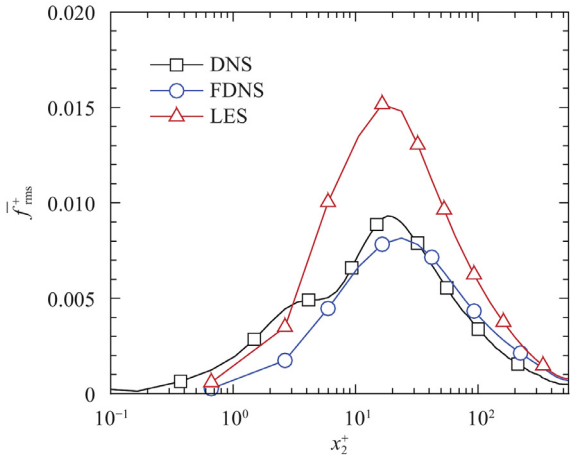

Fig. 2. Profiles of the RMS values of the pressure source term $\bar{f}_{rms}^+$ obtained from DNS, FDNS, and LES.

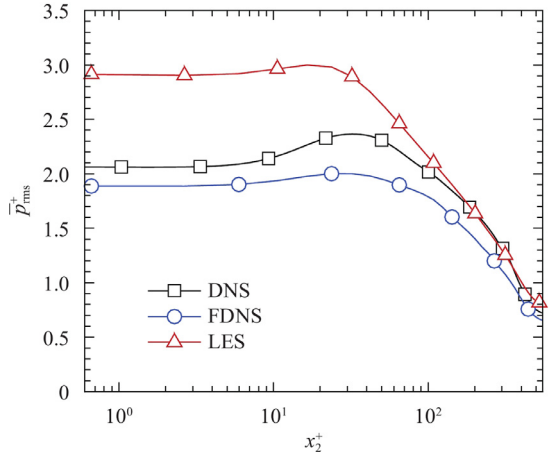

Fig. 3. Profiles of the resolved RMS pressure $\bar{p}_{rms}^+$ obtained from DNS, FDNS, and LES.

out in the FDNS data. In LES, the magnitudes of $\bar{u}_{i,rms}^+$ are overestimated in comparison with the FDNS results, indicating that the dissipation provided by the subgrid-scale model is insufficient in the present LES.

Before we present the results of pressure, its source term f (in DNS, or $\bar{f}$ in FDNS and LES) is first examined. The definitions of f and $\bar{f}$ are given in Eqs. (1)–(3). Figure 2 compares the RMS values of the resolved pressure source terms $\bar{f}_{rms}^+$ obtained from DNS, FDNS, and LES. It is observed that the magnitude of $\bar{f}_{rms}^+$ obtained from FDNS is close to the DNS result. In contrast, the LES overestimates the magnitude of $\bar{f}_{rms}^+$ by approximately 60% in comparison with the DNS result. Noticing that the LES error in $\bar{u}_{i,rms}^+$ is only 10% (Fig. 1b), it is evident that the error in velocity is scale-dependent. Specifically, the error in the velocity fluctuation u_i mainly occurs at small scales, which is amplified by the spatial derivative in the pressure source term. We have also examined the error in each component of the pressure source term. It is found that among all of the six components of $\frac{\partial \bar{u}_i}{\partial x_j}\frac{\partial \bar{u}_j}{\partial x_i}$, the error in $\frac{\partial \bar{u}_1}{\partial x_2}\frac{\partial \bar{u}_2}{\partial x_1}$ is most significant, which reaches 160% approximately and is mainly responsible for the error in the total pressure source term.

Figure 3 compares the profiles of the resolved RMS pressure $\bar{p}_{rms}^+$ obtained from DNS, FDNS, LES. Here, the resolved pressure fluctuation of DNS refers to the solution of Eq. (2), while the FDNS and LES values are obtained by solving Eq. (3) with $\bar{u}_i$ being the resolved velocity of FDNS and LES, respectively. As shown in Fig. 3, the magnitude of the resolved RMS pressure of FDNS is lower than the DNS result. Compared to the FDNS results, the LES overpredicts the magnitude of $\bar{p}_{rms}^+$ in the viscous sublayer for $x_2^+ < 5$, buffer layer for $5 \le x_2^+ < 30$, and part of the logarithmic layer for $x_2^+ < 150$. Particularly, the RMS value of wall pressure is overestimated in LES by approximately 50%. Such an overestimation of $\bar{p}_{rms}^+$ in LES is consistent with the results of the RMS value of the pressure source term shown in Fig. 2.

Figure 4 compares the $k_1-\omega$ spectrum of the wall pressure fluctuation $\Phi_{pp}^+(k_1^+, \omega^+)$ obtained from DNS, FDNS, and LES. To facilitate a quantitative comparison of the results, profiles of $\Phi_{pp}^+(k_1^+, \omega^+)$ as a function of ω^+ at specific streamwise wavenumbers, i.e., $k_1^+ = 0.005, 0.018, 0.036$, are depicted in Fig. 5. From Figs. 4a and 5, it is observed that the FDNS and DNS results are in general consistent near the convective peak, which is located at relatively low streamwise wavenumber $k_1^+ = 0.005$ and frequency $\omega^+ = 0.1$. In the low-value region at larger streamwise wavenumbers or frequencies, the FDNS slightly under-predicts the 'energy' level of the spectrum of the wall pressure fluctuation. In this regard, the filtering only influences the resolved pressure fluctuation near the cut-off wavenumbers and high frequencies, while the small wavenumbers and low frequencies corresponding to large-scale and long-term motions remain almost unchanged. Figures 4b and 5 show that the disagreement between LES and DNS is apparent near the convective peak. The LES overestimates the spectral magnitude of the wall pressure fluctuation.

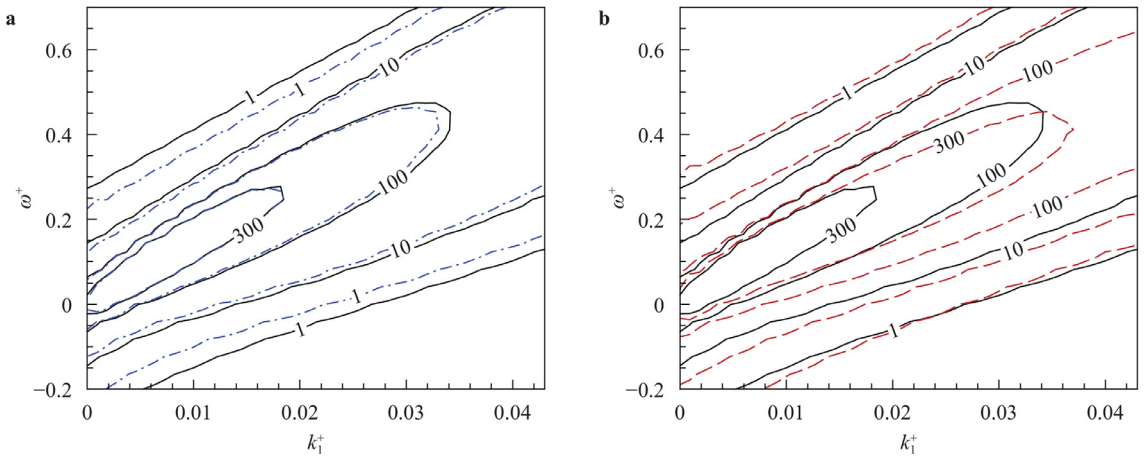

Fig. 4. Isopleths of the $k_1-\omega$ spectrum of the wall pressure fluctuation $\Phi_{pp}^+(k_1^+,\omega^+)$ obtained from **a** DNS and FDNS and **b** DNS and LES. The solid, dash-dotted and dashed lines represent the results of DNS, FDNS and LES, respectively.

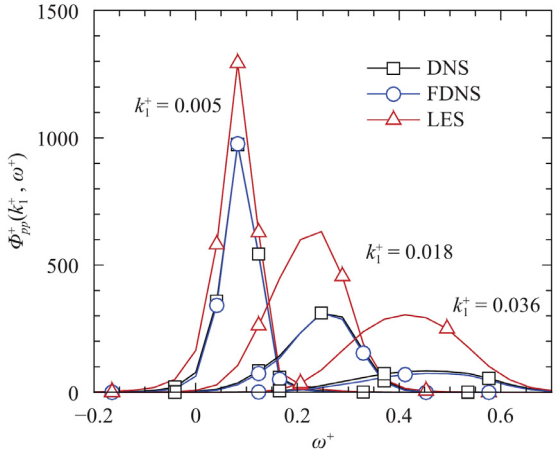

Fig. 5. Profiles of the $k_1-\omega$ spectrum of the wall pressure fluctuation $\Phi_{pp}^+(k_1^+,\omega^+)$ at specific streamwise wavenumbers.

The wavenumber-dependent convective velocity $U_c(k_1)$ and spectral bandwidth $B(k_1)$ are two key indicators of the wavenumber–frequency spectrum, which are defined respectively as [15]:

$$U_c(k_1)=\frac{\int\omega\cdot\Phi(k_1,\omega)\mathrm{d}\omega}{k_1\int\Phi(k_1,\omega)\mathrm{d}\omega}, \tag{9}$$

and

$$B(k_1)=\frac{\int(\omega-U_c(k_1)k_1)^2\cdot\Phi(k_1,\omega)\mathrm{d}\omega}{\int\Phi(k_1,\omega)\mathrm{d}\omega}. \tag{10}$$

Figure 6 compares the values of $U_c(k_1)$ and $B(k_1)$ of the $k_1-\omega$ spectrum of the wall pressure fluctuation obtained from DNS, FDNS, and LES. In consistent with the observations from Figs. 4a and 5, the results of FDNS are in good agreement with those of DNS. From Fig. 6a, it is seen that the convective velocity $U_c(k_1)$ obtained from LES is lower than the DNS and FDNS results, while Fig. 6b shows that the LES under-estimates the spectral bandwidth $B(k_1)$ at high wavenumbers. In the present study, to analyze the error of LES in the wall pressure fluctuation, DNS and LES of a turbulent channel flow at $Re_\tau=550$ are conducted, and FDNS data are obtained by applying a spectral cut-off filter on the DNS data. The RMS pressure and wavenumber–frequency spectrum of the wall pressure fluctuation of FDNS are in general consistent with the DNS results. The filtering operation only influences the resolved pressure near the cut-off scale. In contrast, the LES overestimates both the RMS value and the spectral energy level of the wall pressure fluctuation, indicating that the error in the velocity gradient is the dominant source that induces the error in the wall

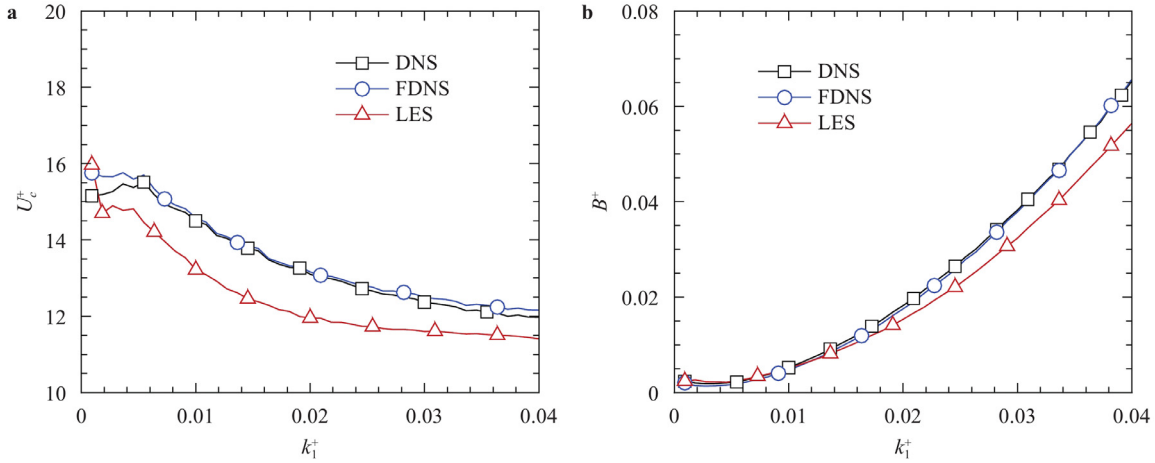

Fig. 6. Wavenumber-dependent **a** convective velocity and **b** spectral bandwidth of the $k_1-\omega$ spectrum of the wall pressure fluctuation.

pressure fluctuation. The results obtained from the present study suggest that improving the accuracy of the velocity gradient is crucial for making better predictions of the wall pressure fluctuation in LES. As a final remark of this paper, we note that the present study focuses on identifying the issue of LES that the error in the wall pressure fluctuation is highly dependent on the error in the velocity fluctuations. This conclusion is drawn based on the test of turbulent channel flow at $Re_\tau = 550$ using specific grid resolution and numerical scheme. In the future, the influences of Reynolds number, grid resolution, and numerical scheme need to be examined systematically to provide a more comprehensive understanding of the problem.

Declaration of Competing Interest

The authors declare that they have no known competing financial interests or personal relationships that could have appeared to influence the work reported in this paper.

Acknowledgements

This research is supported by the National Natural Science Foundation of China (NFSC) Basic Science Center Program for "Multiscale Problems in Nonlinear Mechanics" (Grant 11988102) and the National Key Project (Grant GJXM92579). Shizhao Wang acknowledges the support from the National Natural Science Foundation of China (Grant 11922214).

References

[1] W.K. Blake, Mechanics of Flow-Induced Sound and Vibration, Academic Press, 1986.
[2] M. Wang, J.B. Freund, S.K. Lele, Computational prediction of flowgenerated sound, Annu. Rev. Fluid Mech. 38 (2006) 483–512.
[3] W.W. Willmarth, Pressure fluctuations beneath turbulent boundary layers, Annu. Rev. Fluid Mech. 7 (1975) 13–36.
[4] H. Eckelmann, A review of knowledge on pressure fluctuations, in: Near-Wall Turbulence: 1988 Zoran Zaric Memorial Conference, (ed. Kline, S. J. & Afgan, N. H.), Hemisphere, 1989, pp. 328–347.
[5] J. Kim, On the structure of pressure fluctuations in simulated turbulent channel flow, J. Fluid Mech. 205 (1989) 421–451.
[6] H. Choi, P. Moin, On the space-time characteristics of wall-pressure fluctuations, Phys. Fluids A: Fluid Dyn. 2 (1990) 1450–1460.
[7] P.A. Chang, U. Piomelli, W.K. Blake, Relationship between wall pressure and velocity-field sources, Phys. Fluids 11 (1999) 3434–3448.
[8] Z.W. Hu, C.L. Morfey, N.D. Sandham, Wall pressure and shear stress spectra from direct simulations of channel flow, AIAA J. 44 (2006) 1541–1549.
[9] S.B. Pope, in: Direct Numerical Simulation, Cambridge University Press, 2000, pp. 344–357.
[10] S. Viazzo, A. Dejoan, R. Schiestel, Spectral features of the wall-pressure fluctuations in turbulent wall flows with and without perturbations using LES, Int. J. Heat Fluid Flow 22 (2001) 39–52.
[11] G.I. Park, P. Moin, Space-time characteristics of wall-pressure and wall shear-stress fluctuations in wall-modeled large eddy simulation, Phys. Rev. Fluids 1 (2016) 024404.
[12] G.E. Karniadakis, M. Israeli, S.A. Orszag, High-order splitting methods for the incompressible Navier–Stokes equations, J. Comput. Phys. 97 (1991) 414–443.
[13] M. Germano, U. Piomelli, P. Moin, et al., A dynamic subgrid-scale eddy viscosity model, Phys. Fluids A: Fluid Dyn. 3 (1991) 1760–1765.
[14] D.K. Lilly, A proposed modification of the germano subgrid-scale closure method, Phys. Fluids A: Fluid Dyn. 4 (1992) 633–635.
[15] T. Wu, C. Geng, Y. Yao, et al., Characteristics of space-time energy spectra in turbulent channel flows, Phys. Rev. Fluids 2 (2017) 084609.